GEOMETRIC TUNING OF ENERGY STORAGE IN BARIUM TITANATE/STRONTIUM TITANATE NANOCOMPOSITES

Ha Thi Dang[1,2], Dang Thi Hong Hue[3], Ba-Hieu Vu[3], Trong-Giang Nguyen[3], Van-Hai Dinh[3], Le Van Lich[3]*

[1]Vietnam National University of Forestry, Hanoi, Vietnam
[2]PhD student in Materials Engineering, Hanoi University of Science and Technology, Hanoi, Vietnam
[3]Hanoi University of Science and Technology, Hanoi, Vietnam

*Corresponding author: lich.levan@hust.edu.vn

(Received: April 29, 2025; Revised: June 15, 2025; Accepted: June 20, 2025)

DOI: 10.31130/ud-jst.2025.23(10B).641E

Abstract - This study employs phase-field simulations to systematically investigate the impact of barium titanate nanoparticle geometry on polarization domain structures and energy storage properties in barium titanate/strontium titanate nanocomposites. Results reveal distinct polarization domain configurations, including dominant *c* domains in nanowire-based composites, coexisting a_1/a_2 and *c* domains with comparable fractions in nanodot systems, and a near-absence of *c* domains in nanodisk geometries. These variations of domain structures give rise to divergent hysteresis behaviors, where nanowire composites exhibit large hysteresis loops, nanodot systems display narrower loops, and nanodisk configurations show negligible hysteresis behavior. Notably, transitioning barium titanate geometry from nanowires to nanodisks significantly enhances discharge energy density and energy efficiency, attributed to optimized domain dynamics. The findings propose a novel strategy for improving energy storage capacity in ferroelectric/paraelectric nanocomposites through geometric engineering of the ferroelectric phase to regulate polarization domain structures.

Key words – Energy storage property; Ferroelectric/paraelectric nanocomposite; Domain structure; Phase field model.

1. Introduction

The accelerated expansion of environmentally sustainable energy technologies has generated substantial demand for electronic devices exhibiting advanced energy storage capabilities [1-3]. This technological evolution has intensified focus on optimizing energy density capacity and improving power conversion effectiveness, driving considerable scientific investigation. Within this context, dielectric capacitors have emerged as critical elements in modern pulsed power systems, distinguished by their ultrahigh power density capabilities and rapid charge-discharge cycles [4, 5], characteristics that position them advantageously against alternative storage solutions like battery systems and electrochemical capacitors. Recent research has prioritized ferroelectric ceramic dielectrics, which demonstrate elevated dielectric constants through spontaneous polarization mechanisms, coupled with outstanding durability against fatigue and stable thermal characteristics [6]. Nevertheless, traditional ferroelectric materials exhibit intrinsic limitations, including constrained dielectric strength and significant polarization-field hysteresis loops that impede optimal energy storage functionality. These challenges underscore the necessity for strategic material engineering of conventional ferroelectric systems to enable their adaptation for high-performance energy storage applications.

Recent research identifies two principal methodologies for optimizing dielectric energy storage materials, including microstructural refinement through grain dimension control and polarization domain engineering [7-10]. Microstructural optimization via grain size reduction demonstrates improved dielectric strength, directly correlating with enhanced energy storage capacity [11, 12]. Parallel development focuses on transforming conventional ferroelectrics into relaxor variants through atomic-scale modifications, where strategic doping and solid solution techniques disrupt macro-scale polarization structures into localized nano-ordered states [13-16]. This nanoconfinement effect reduces inter-domain coupling forces and minimizes polarization reversal energy barriers, significantly improving energy discharge density while maintaining operational efficiency [17, 18]. For example, an experimental study shows lanthanum-modified PZT systems achieving 85 J/cm³ storage density with 65% efficiency at 4.5 MV/cm through such domain engineering [19]. Advanced multicomponent solid-solution architectures leverage heterogeneous nanodomain configurations (rhombohedral/tetragonal phases in cubic matrices) to reach 112 J/cm³ at 4.9 MV/cm with 85% efficiency [20]. Targeted defect engineering through ionic implantation in PMN-PT systems elevates performance to 133 J/cm³ under 5.9 MV/cm electrical stress [21]. Furthermore, a recent approach employs nanoscale polar configurations to eliminate hysteresis losses while preserving polarization intensity, realizing breakthrough metrics of 152 J/cm³ storage density with 90% efficiency at reduced 3.5 MV/cm operational fields [22].

While considerable advancements in energy storage optimization have been achieved via microstructural refinement and domain engineering, current investigations predominantly emphasize dielectric breakdown strengths for high-field endurance [23]. However, emerging applications in miniaturized electronics and integrated systems necessitate dielectric capacitors with superior low-voltage operational capabilities [24]. Recent efforts have addressed this paradigm shift by incorporating functional additives to modulate relaxation dynamics and

domain architectures, enabling efficient energy storage under reduced electric fields [24–30]. This transition emphasizes the critical need for developing ferroelectric systems optimized for low-voltage environments without compromising storage capacity.

This study systematically examines the energy storage characteristics of ferroelectric/paraelectric $BaTiO_3/SrTiO_3$ (BTO/STO) nanocomposites through computational modeling. The focus of this study is on the effect of BTO nanoparticle geometry embedded in STO matrix on the domain structures and energy storage properties. Three types of BTO nanoparticle geometry are considered, including nanowires, nanodots, and nanodisks. Phase-field simulations elucidate domain configuration evolution and polarization-electric field hysteresis, while derived *P-E* loop analyses enable quantitative assessment of discharge energy density and conversion efficiency.

2. Methodology

2.1. Free energy of $BaTiO_3/SrTiO_3$ nanocomposites

To investigate domain structures and energy storage capacities of ferroelectric/paraelectric BTO/STO nanocomposites, a phase-field model is developed. The model employs the polarization vector $P(p_1, p_2, p_3)$ to characterize domain configurations and their evolution under external fields. The total energy H of BTO/STO nanocomposites is calculated by integrating the total energy density h over the entire volume of the system V as follows:

$$H = \int h dV = \int [(1-f)h^{BTO} + f h^{STO}] dV \quad (1)$$

where f is a parameter used to define composite phases, specifically, f = 0 and 1 correspond to the BTO and STO materials, respectively. In Eq. (1), the total energy densities of BTO and STO phases are denoted as h^{BTO} and h^{STO}, respectively. The total energy density of BTO consists of Landau, elastic, gradient energy, and electric densities, i.e.,

$$h^{BTO} = h^{BTO}_{Landau} + h^{BTO}_{Elastic} + h^{BTO}_{Gradient} + h^{BTO}_{Electric} \quad (2)$$

Similarly, the total energy density of STO comprises Landau, elastic, gradient energy, and electric densities, which can be expressed as

$$h^{STO} = h^{STO}_{Landau} + h^{STO}_{Elastic} + h^{STO}_{Gradient} + h^{STO}_{Electric} \quad (3)$$

Detailed expressions of energy density components are provided in the previous study [31].

2.2. The equilibrium and governing equations

The equilibrium condition for the mechanical field is expressed as

$$\nabla \cdot \sigma = \frac{\partial}{\partial x_j}\left(\frac{\partial h}{\partial \varepsilon_{ij}}\right) = 0 \quad (4)$$

The electric equilibrium is described by

$$\epsilon_0 \epsilon^b_{ij} \nabla_i \nabla_j \phi = p_{i,i}, \quad (5)$$

where ϕ, ϵ_0, and ϵ^b_{ij} are the electrostatic potential, the vacuum permittivity, and the relative background permittivity, respectively. The temporal polarization evolution can be described by solving the time-dependent Ginzburg–Landau equation, as

$$\frac{\partial p_i(x_j,t)}{\partial t} = -M \frac{\delta H}{\delta p_i(x_j,t)} \quad (6)$$

where M and t are the mobility coefficient and the evolution time, respectively.

2.3. Simulation models and procedures

In this study, ferroelectric/paraelectric BTO/STO nanocomposites are investigated. The nanocomposites consist of BTO nanoparticles embedded in an STO matrix. Three types of BTO geometries are considered, including nanowires, nanodots, and nanodisks, as shown in Figure 1. Our investigation focuses on studying the effect of ferroelectric geometries on domain structures and energy storage performance. The solid volume fraction of BTO nanoparticles is fixed at 60 %. The dimensions of BTO nanoparticles are 16×16×128 nm for nanowires, 32×32×32 nm for nanodots, and 64×64×8 nm for nanodisks. Note that extensive experimental research has successfully fabricated ferroelectric-paraelectric nanocomposites [32–36]. These methodologies include techniques like the solvothermal process [32], hydrothermal method [33, 34], sol-precipitation [35], and high-pressure rapid field-assisted sintering [36]. By precisely controlling growth parameters, the synthesis of the intended architecture is achievable, integrating ferroelectric nanoparticles into the paraelectric matrix.

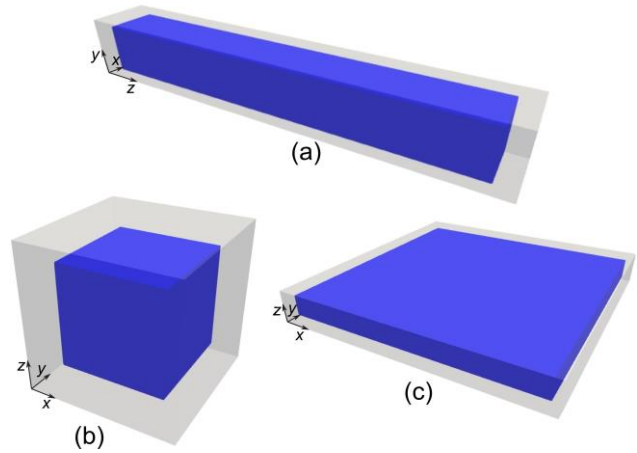

Figure 1. *Schematic illustrations of $BaTiO_3/SrTiO_3$ nanocomposites with different nanoparticle geometries: (a) 16×16×128 nm nanowire, (b) 32×32×32 nm nanodot, and (c) 64×64×8 nm nanodisk*

To discretize the system, regular grid points with the grid size Δx=Δy=Δz=0.4 nm are employed. The coordinate axes x, y, and z correspond to the [100], [010], and [001] crystalographic orientations, respectively. Periodic boundary conditions are applied in all three major directions. The material properties of BTO and STO are adopted from previous studies [32, 37]. The phase-field simulations are performed at room temperature. The equilibrium domain structures of nanocomposites are determined by iteratively solving the time-dependent Ginzburg–Landau equation, starting from an initial polarization setup with small random fluctuations and advancing through a sufficient number of time steps until the total free energy converges. The temporal iteration of the time-dependent Ginzburg–

Landau equation is performed using the semi-implicit Fourier spectral method [33,34]. After establishing the polarization configuration at thermodynamic equilibrium, we apply a vertical quasi-static electric field in the *z* direction to observe the polarization behavior and switching.

3. Results and discussion

3.1. Polarization domain structures

Domain structures formed in nanocomposites with different nanoparticle geometries are shown in Figure 2. It can be seen from Figure 2a that for a nanowire with a size of 16×16×128 nm, the domain structure includes many *c* domains (domains with polarization aligned in the *z* direction) and a few a_1/a_2 domains (domains in the *xy* plane). In a nanowire with an axial dimension much longer than the lateral length, the effect of lateral stress arising from the geometry plays an important role in determining the domain structures, thus, the nanowire favors many *c* domains and a few a_1/a_2 domains, as shown in Figure 2a. The preferential formation of c-domains in such nanowires can be attributed to a combination of factors, including lateral mechanical confinement, suppression of depolarization fields, and electrostatic and elastic boundary conditions imposed by the surrounding paraelectric STO matrix. Specifically, the nanowire experiences lateral compressive stress within the ferroelectric BTO core due to its confinement by the STO matrix. Lateral compressive stress in the *x*- and *y*-directions energetically favors polarization along the vertical (*z*) axis. As a result, the formation of out-of-plane c-domains becomes thermodynamically preferred. This is consistent with previous studies which demonstrated that compressive in-plane strain promotes the stabilization with out-ofplane polarization [38]. Similar polarization behavior has also been reported in previous studies on single-crystal ferroelectric nanowires [39, 40]. In a nanodot with a size equal to 32×32×32 nm, the a_1/a_2 and *c* domains coexist with similar volume fractions, as shown in Figure 2b. Domains assemble into vortex domain structures in the nanodot, which has also been observed experimentally [38] and verified by first-principle calculations [39]. With further decreases in the aspect ratio, *c* domains disappear, and a_1/a_2 twin domains and some in-plane vortex domains become stable, as shown in Figure 2c. In nanodisks with significantly reduced thickness along the *z*-direction compared to their lateral dimensions, geometric constraints intensify the influence of depolarization fields along the *z*-axis. These depolarization fields arise due to the broken periodicity and incomplete screening of surface charges at the BTO/STO interfaces, which become more pronounced as the ferroelectric layer thickness is reduced [40]. Such fields energetically penalize out-of-plane polarization, destabilizing *c*-domains and favoring in-plane polarization components. As a result, the polarization vectors tend to reorient within the plane of the nanodisk, leading to the formation of a_1/a_2 twin domains and the stabilization of in-plane vortex domain structures. This domain reconfiguration reflects a topological transition governed by geometric scaling and electrostatic boundary conditions, which suppress the out-of-plane polarization component and promote in-plane domain order. Note that the polarization absences in the STO paraelectric matrix.

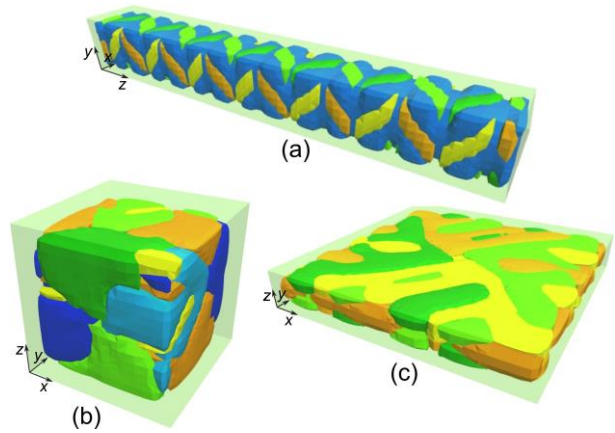

Figure 2. *Domain structures of $BaTiO_3/SrTiO_3$ nanocomposites with different nanoparticle geometries: (a) 16×16×128 nm nanowire, (b) 32×32×32 nm nanodot, and (c) 64×64×8 nm nanodisk. Yellow, orange, light green, dark green, light blue, and dark blue indicate domain structures with polarization along the [100], [-100], [010], [0-10], [001], and [00-1] directions, respectively*

3.2. Polarization switching and energy-storage performance of BTO/STO nanocomposites

Figure 3 presents the polarization-electric field (P_3-E_3) hysteresis loops for BTO/STO nanocomposites with different geometries of BTO nanoparticles. For the nanocomposite with BTO nanowires, the material exhibits a broad and rectangular-shaped profile of hysteresis loop, indicative of a well-defined ferroelectric behavior with a substantial remanent polarization. This behavior mainly results from the predominance of *c* domains, whose polarization vectors align effectively with the external electric field, facilitating strong and reliable dipole switching [41]. However, for the nanocomposite with BTO nanodots, the P_3-E_3 loop becomes narrower and more slanted, suggesting a weakened ferroelectric behavior with a reduced remanent polarization and decreased coercive field. This reduction is caused by the coexistence of *c* and a_1/a_2 domains, resulting in less effective polarization alignment and partial dipole switching. When the BTO nanoparticles adopt a nanodisk geometry characterized by a low aspect ratio, the hysteresis loop disappears, and the P_3-E_3 behavior is similar to that of nonlinear paraelectric materials. This trend in polarization-electric field behaviors can be attributed to the transition of polarization domain structures as the BTO nanoparticles change their geometries from nanowire to nanodisk. More specifically, the large volume fraction of *c* domains in the nanocomposite with BTO nanowires facilitates the large remanent polarization, such that resulting in a large hysteresis loop. In contrast, the low volume fraction of *c* domains in the nanocomposite with BTO nanodisks gives rise to small or even zero remanent polarization, bringing about the disappearance of the hysteresis loop. Therefore, the change in BTO geometries can tailor the polarization-

electric field behavior of the BTO/STO nanocomposites. This finding emphasizes the ability to tailor the ferroelectric properties of BTO/STO nanocomposites by engineering the morphology of embedded ferroelectric nanoparticles, which directly impacts the domain configuration and electromechanical performance.

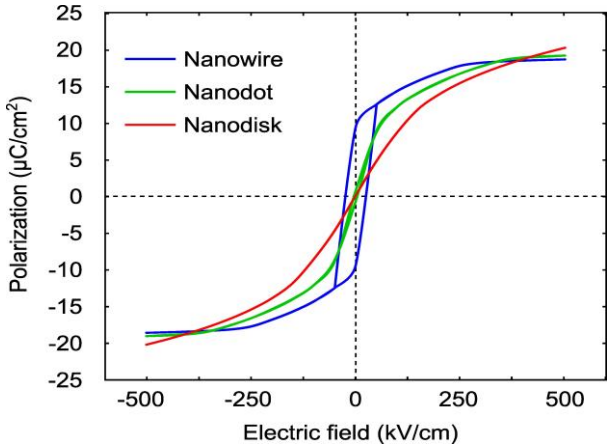

Figure 3. *Polarization-electric field behaviors of $BaTiO_3/SrTiO_3$ nanocomposites with different nanoparticle geometries at room temperature under an applied electric field of 500 kV/cm*

Figure 4 shows the dependence of both the maximum polarization (P_{max}) at E_3 = 500 kV/cm and the remanent polarization (P_r) at zero electric field on the BTO geometry. These values are determined by analyzing the P_3-E_3 behaviors of BTO/STO nanocomposites, as shown in Figure 3. Interestingly, while the maximum polarization P_{max} values slightly decrease with the change of BTO geometry, the remanent polarization P_r experiences a significant decrease and reaches almost zero for the nanocomposite with BTO nanodisks. The similar magnitude of P_{max} can be attributed to the same volume fraction of BTO nanoparticles in the nanocomposites. In addition, the difference between maximum and remanent polarization, i.e., $\Delta P = P_{max} - P_r$, is also included in Figure 4. Notably, the magnitude of ΔP increases when the BTO nanoparticles change their geometries from nanowire to nanodisk. The previous study [31] suggests that the large difference between maximum and remanent polarizations is beneficial for discharge storage energy density.

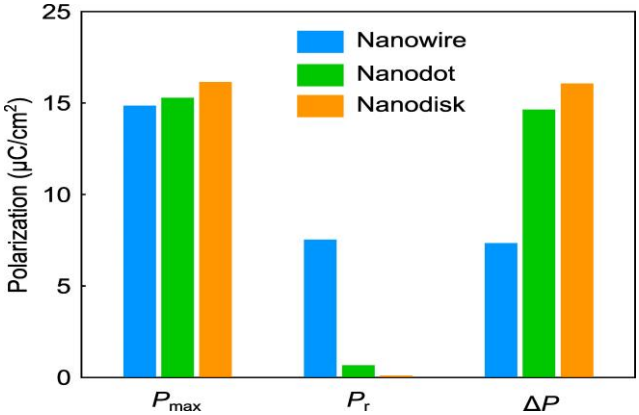

Figure 4. *Dependence of the maximum polarization and the remanent polarization on the geometries of $BaTiO_3/SrTiO_3$ nanocomposites*

Next, the energy storage performance of BTO/STO nanocomposites is considered. Theoretically, the energy storage performance can be evaluated by

$$U_c = \int_0^{p_{max}} Edp \quad (7)$$

$$U_d = \int_{p_r}^{p_{max}} Edp \quad (8)$$

$$\eta = \frac{U_d}{U_c} \times 100\% \quad (9)$$

where U_c, U_d, and η represent the charge energy storage density, the discharge energy storage density, and the charge–discharge efficiency, respectively. In ferroelectric capacitors, the large P_3-E_3 hysteresis loop results in inevitable energy loss ($U_{loss} = U_c - U_d$). As a result, an important parameter called energy efficiency (η) reflects the effective utilization of energy storage. The energy density is primarily determined by the electrical polarization, breakdown strength, and hysteresis loop.

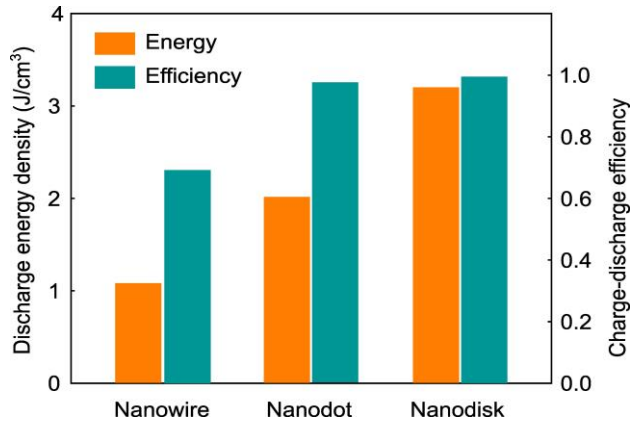

Figure 5. *Discharge energy density and charge–discharge efficiency of $BaTiO_3/SrTiO_3$ nanocomposites with different geometries*

Figure 5 illustrates the dependence of discharge energy density on the geometry of BTO nanoparticles when the nanocomposites are recovered from poled states by an electric field of 500 kV/cm. Both discharge energy density and energy efficiency increase when the BTO nanoparticles change their geometries from nanowire to nanodisk. Particularly, the nanocomposite with BTO nanowires achieves the discharge energy density of 1.08 J/cm^3 and a low efficiency of 70 %. The nanocomposite with BTO nanodots achieves the discharge energy density of 2.01 J/cm^3 and efficiency of 98 %. Finally, the nanocomposite with BTO nanodisks achieves the discharge energy density of 3.22 J/cm^3 and efficiency of 100 %. The magnitude of discharge energy density for BTO nanodisks is three times higher than that for BTO nanowires. The enhanced discharge energy density and efficiency arise from the narrow hysteresis behavior exhibited by the nanocomposite with BTO nanodisks. This remarkable enhancement highlights the critical role of morphological engineering in tailoring the energy storage performance of ferroelectric-paraelectric nanocomposites. By leveraging this geometry-dependent mechanism, future design strategies can target specific domain configurations-such as vortex or a_1/a_2 twin domains-to optimize dielectric and energy storage properties in nanoscale ferroelectric systems.

4. Conclusion

In summary, this study reveals a significant effect of BTO nanoparticle geometry on domain structures and energy storage performance in BTO/STO nanocomposites through phase-field simulations. Nanocomposites with BTO nanowires primarily exhibit *c* domains, while those with nanodisks show nearly complete suppression of *c* domains. In contrast, nanodot-based systems display coexisting a_1/a_2 and *c* domains with comparable volume fractions. These structural differences produce distinct hysteresis behaviors, where nanowire composites exhibit large hysteresis loops that progressively narrow in nanodot systems and vanish entirely in nanodisk configurations. Crucially, transitioning from nanowires to nanodisks enhances discharge energy density (from 1.08 to 3.22 J/cm^3) and energy efficiency (70% to 100%). These findings demonstrate that geometric engineering of ferroelectric phases in nanocomposites enables strategic control of polarization domain architectures, providing a promising pathway for developing high-performance dielectric energy storage systems.

Acknowledgments: This research is funded by Vietnam National Foundation for Science and Technology Development (NAFOSTED) under Grant Number 103.02–2021.79.

REFERENCES

[1] H.D. Yoo, E. Markevich, G. Salitra, D. Sharon, and D. Aurbach, "On the challenge of developing advanced technologies for electrochemical energy storage and conversion", *Materials today*, vol. 17, no. 3, pp. 110-121, 2014. https://doi.org/10.1016/j.mattod.2014.02.014

[2] Y. Huang *et al.*, "Multifunctional energy storage and conversion devices", *Advanced Materials*, vol. 28, no. 38, pp. 8344-8364, 2016. https://doi.org/10.1002/adma.201601928

[3] S.L. Candelaria *et al.*, "Nanostructured carbon for energy storage and conversion", *Nano energy*, vol. 1, no. 2, pp. 195-220, 2012. https://doi.org/10.1016/j.nanoen.2011.11.006

[4] H. Palneedi, M. Peddigari, G. T. Hwang, D. Y. Jeong, and J. Ryu, "High-performance dielectric ceramic films for energy storage capacitors: progress and outlook", *Advanced Functional Materials*, vol. 28, no. 42, pp. 1803665, 2018. https://doi.org/10.1002/adfm.201803665

[5] L. Yang *et al.*, "Perovskite lead-free dielectrics for energy storage applications", *Progress in Materials Science*, vol. 102, pp. 72-108, 2019. https://doi.org/10.1016/j.pmatsci.2018.12.005

[6] H. Huang and J.F. Scott, *Ferroelectric materials for energy applications*, John Wiley & Sons, 2018.

[7] Z. Lu *et al.*, "Mechanism of enhanced energy storage density in $AgNbO_3$-based lead-free antiferroelectrics", *Nano Energy*, vol. 79, pp. 105423, 2021. https://doi.org/10.1016/j.nanoen.2020.105423

[8] Z. Lu *et al.*, "Superior energy density through tailored dopant strategies in multilayer ceramic capacitors", *Energy Environmental Science*, vol. 13, no. 9, pp. 2938-2948, 2020. DOI: 10.1039/D0EE02104K

[9] H. Ji *et al.*, "Ultrahigh energy density in short-range tilted NBT-based lead-free multilayer ceramic capacitors by nanodomain percolation", *Energy Storage Materials*, vol. 38, pp. 113-120, 2021. https://doi.org/10.1016/j.ensm.2021.01.023

[10] H. Ye *et al.*, "Significantly improvement of comprehensive energy storage performances with lead-free relaxor ferroelectric ceramics for high-temperature capacitors applications", *Acta Materialia*, vol. 203, pp. 116484, 2021. https://doi.org/10.1016/j.actamat.2020.116484

[11] J. Chen, H. Qi, and R. Zuo, "Realizing Stable Relaxor Antiferroelectric and Superior Energy Storage Properties in $(Na_{1-x/2}La_{x/2})(Nb_{1-x}Ti_x)O_3$ Lead-Free Ceramics through A/B-Site Complex Substitution", *ACS Applied Materials Interfaces*, vol. 12, no. 29, pp. 32871-32879, 2020. https://doi.org/10.1021/acsami.0c09876

[12] Z. Yang *et al.*, "Grain size engineered lead-free ceramics with both large energy storage density and ultrahigh mechanical properties", *Nano Energy*, vol. 58, pp. 768-777, 2019. https://doi.org/10.1016/j.nanoen.2019.02.003

[13] H. Pan *et al.*, "Giant energy density and high efficiency achieved in bismuth ferrite-based film capacitors via domain engineering", *Nature communications*, vol. 9, no. 1, pp. 1813, 2018. https://doi.org/10.1038/s41467-018-04189-6

[14] H. Qi, A. Xie, A. Tian, and R. Zuo, "Superior energy-storage capacitors with simultaneously giant energy density and efficiency using nanodomain engineered $BiFeO_3$-$BaTiO_3$-$NaNbO_3$ lead-free bulk ferroelectrics", *Advanced Energy Materials*, vol. 10, no. 6, pp. 1903338, 2020. https://doi.org/10.1002/aenm.201903338

[15] Q. Wang *et al.*, "$Bi_{0.5}Na_{0.5}TiO_3$-based relaxor-ferroelectric ceramics for low-electric-field dielectric energy storage via bidirectional optimization strategy", *Chemical Engineering Journal*, vol. 452, pp. 139422, 2023. https://doi.org/10.1016/j.cej.2022.139422

[16] Q. Zheng, B. Xie, Y. Tian, Q. Wang, H. Luo, Z. Liu, and H. Zhang, "High recoverable energy density of Na0. 5Bi0. 5TiO3-based ceramics by multi-scale insulation regulation and relaxor optimization strategy", *Journal of Materiomics*, vol. 10, no. 4, pp. 845-856, 2024. https://doi.org/10.1016/j.jmat.2023.10.005

[17] H. Pan, A. Kursumovic, Y.-H. Lin, C.-W. Nan, and J. L. MacManus-Driscoll, "Dielectric films for high performance capacitive energy storage: multiscale engineering", *Nanoscale*, vol. 12, no. 38, pp. 19582-19591, 2020. DOI: 10.1039/D0NR05709F

[18] X. Lv, X.-x. Zhang, and J. Wu, "Nano-domains in lead-free piezoceramics: a review", *Journal of Materials Chemistry A*, vol. 8, no. 20, pp. 10026-10073, 2020. https://doi.org/10.1039/D0TA03201H

[19] B. Ma, Z. Hu, R.E. Koritala, T.H. Lee, S.E. Dorris, and U. Balachandran, "PLZT film capacitors for power electronics and energy storage applications", *Journal of Materials Science: Materials in Electronics*, vol. 26, no. 12, pp. 9279-9287, 2015. https://doi.org/10.1007/s10854-015-3025-0

[20] H. Pan *et al.*, "Ultrahigh–energy density lead-free dielectric films via polymorphic nanodomain design", *Science*, vol. 365, no. 6453, pp. 578-582, 2019. DOI: 10.1126/science.aaw8109

[21] J. Kim *et al.*, "Ultrahigh capacitive energy density in ion-bombarded relaxor ferroelectric films", *Science*, vol. 369, no. 6499, pp. 81-84, 2020. DOI: 10.1126/science.abb0631

[22] H. Pan *et al.*, "Ultrahigh energy storage in superparaelectric relaxor ferroelectrics", *Science*, vol. 374, no. 6563, pp. 100-104, 2021. DOI: 10.1126/science.abi7687

[23] J. Cai *et al.*, "Design and preparation of ternary polymer nanocomposites for high energy density film capacitors", *Composites Science Technology*, vol. 245, pp. 110361, 2024. https://doi.org/10.1016/j.compscitech.2023.110361

[24] R. Kang *et al.*, "Domain engineered lead-free ceramics with large energy storage density and ultra-high efficiency under low electric fields", *ACS Applied Materials Interfaces*, vol. 13, no. 21, pp. 25143-25152, 2021. https://doi.org/10.1021/acsami.1c05824

[25] D. Zheng, R. Zuo, D. Zhang, and Y. Li, "Novel BiFeO3–BaTiO3–Ba (Mg1/3Nb2/3) O3 lead-free relaxor ferroelectric ceramics for energy-storage capacitors", *Journal of the American Ceramic Society*, vol. 98, no. 9, pp. 2692-2695, 2015. https://doi.org/10.1111/jace.13737

[26] D. Zheng and R. Zuo, "Enhanced energy storage properties in $La(Mg_{1/2}Ti_{1/2})O_3$-modified $BiFeO_3$-$BaTiO_3$ lead-free relaxor ferroelectric ceramics within a wide temperature range", *Journal of the European Ceramic Society*, vol. 37, no. 1, pp. 413-418, 2017. https://doi.org/10.1016/j.jeurceramsoc.2016.08.021

[27] Q. Hu, L. Jin, T. Wang, C. Li, Z. Xing, and X. Wei, "Dielectric and temperature stable energy storage properties of $0.88BaTiO_3$–$0.12Bi(Mg_{1/2}Ti_{1/2})O_3$ bulk ceramics", *Journal of Alloys Compounds*, vol. 640, pp. 416-420, 2015.

https://doi.org/10.1016/j.jallcom.2015.02.225

[28] M. Peddigari *et al.*, "Boosting the recoverable energy density of lead-free ferroelectric ceramic thick films through artificially induced quasi-relaxor behavior", *ACS applied materials interfaces*, vol. 10, no. 24, pp. 20720-20727, 2018. https://doi.org/10.1021/acsami.8b05347

[29] Z. Yang *et al.*, "Significantly enhanced recoverable energy storage density in potassium–sodium niobate-based lead free ceramics", *Journal of materials chemistry A*, vol. 4, no. 36, pp. 13778-13785, 2016. https://doi.org/10.1039/C6TA04107H

[30] T. Shao *et al.*, "Potassium–sodium niobate based lead-free ceramics: novel electrical energy storage materials", *Journal of Materials Chemistry A*, vol. 5, no. 2, pp. 554-563, 2017. https://doi.org/10.1039/C6TA07803F

[31] B.-H. Vu, D.T.H. Hue, T. Shimada, V.-H. Dinh, and M.-H. Phan, "Low-field energy storage enhancement in ferroelectric/paraelectric $PbTiO_3/SrTiO_3$ nanocomposites near antiferroelectric–ferroelectric transition region", *Journal of Science: Advanced Materials Devices*, vol. 9, no. 2, pp. 100687, 2024. https://doi.org/10.1016/j.jsamd.2024.100687

[32] N. Pertsev, A. Tagantsev, and N. Setter, "Phase transitions and strain-induced ferroelectricity in $SrTiO_3$ epitaxial thin films", *Physical review B*, vol. 61, no. 2, pp. R825, 2000. https://doi.org/10.1103/PhysRevB.61.R825

[33] J. Wang, X. Ma, Q. Li, J. Britson, and L.-Q. Chen, "Phase transitions and domain structures of ferroelectric nanoparticles: Phase field model incorporating strong elastic and dielectric inhomogeneity", *Acta materialia*, vol. 61, no. 20, pp. 7591-7603, 2013. https://doi.org/10.1016/j.actamat.2013.08.055

[34] H. T. Dang and V.-H. Dinh, "Polar toron structure in ferroelectric core-shell nanoparticles", *Scripta Materialia*, vol. 236, pp. 115641, 2023. https://doi.org/10.1016/j.scriptamat.2023.115641

[35] A. Schilling *et al.*, "Domains in ferroelectric nanodots", *Nano Letters*, vol. 9, no. 9, pp. 3359-3364, 2009. https://doi.org/10.1021/nl901661a

[36] S. Prosandeev and L. Bellaiche, "Characteristics and signatures of dipole vortices in ferroelectric nanodots: First-principles-based simulations and analytical expressions", *Physical Review B-Condensed Matter Materials Physics*, vol. 75, no. 9, pp. 094102, 2007. https://doi.org/10.1103/PhysRevB.75.094102

[37] Y.H. Huang *et al.*, "Thermodynamic and phase-field studies of phase transitions, domain structures, and switching for $Ba(Zr_xTi_{1-x})O_3$ solid solutions", *Acta Materialia*, vol. 186, pp. 609-615, 2020. https://doi.org/10.1016/j.actamat.2020.01.019

[38] J.-J. Wang, Y.-J. Su, B. Wang, J. Ouyang, Y.-H. Ren, and L.-Q. Chen, "Strain engineering of dischargeable energy density of ferroelectric thin-film capacitors", *Nano Energy*, vol. 72, pp. 104665, 2020. https://doi.org/10.1016/j.nanoen.2020.104665

[39] A. Schilling, R. Bowman, G. Catalan, J. Scott, and J. Gregg, "Morphological control of polar orientation in single-crystal ferroelectric nanowires", *Nano letters*, vol. 7, no. 12, pp. 3787-3791, 2007. https://doi.org/10.1021/nl0722601

[40] J. Hong, G. Catalan, D. Fang, E. Artacho, and J. Scott, "Topology of the polarization field in ferroelectric nanowires from first principles", *Physical Review B—Condensed Matter Materials Physics*, vol. 81, no. 17, pp. 172101, 2010. https://doi.org/10.1103/PhysRevB.81.172101

[41] J.F. Ihlefeld, D.T. Harris, R. Keech, J. L. Jones, J. P. Maria, and S. Trolier-McKinstry, "Scaling effects in perovskite ferroelectrics: fundamental limits and process-structure-property relations", *Journal of the American Ceramic Society*, vol. 99, no. 8, pp. 2537-2557, 2016. https://doi.org/10.1111/jace.14387